

# 1 Authors' response

**++ overall comment ++ associate editor:** Nice paper and very interesting! However, what the paper title and abstract promise is not fully delivered in the paper. It is very interesting work but the paper seems to be more about the DIC method and measurement campaign and less about the validation. It provides an example of how comparison and validation can be done but not sufficient for a journal article on that specific topic. Generally, there should be a strong explanation for why only one time period of 5 minutes was used. Even two different time periods would bolster the analysis much more strongly.

**Authors' response #1:** Thank you for your detailed feedback. We have reformulated and clarified the abstract and introduction to introduce the novelty of this paper in comparison with the state of the art, which then justifies the presentation of an example of a comparison and validation based on one 5 minute time period. As DIC is a novel method for the detection of rotor blade deformation in the field, this technique is currently in development with potential for improvement. For example, the turbine needs to be in a stable yaw direction, which limits the length of a single time series. DIC as a new measurement method, which is currently in development and shows very promising potential for the validation of aeroelastic codes. The validation of codes based on more time series and more detailed simulations is explained in the outlook-section at the end of the paper and is subject of current investigations.

**++ detailed comment #1 ++ associate editor:** Abstract is too long. Consider shortening and focus on key contributions. The abstract is not a place to provide background and introduction nor future work. The second paragraph has some repetitive content to the first.

**Authors' response #2:** We agree with you and shortened the abstract according to your suggestion.

**++ detailed comment #2 ++ associate editor:** Opening statement not substantiated by a reference. Slightly odd in wording. Why does reduce LCOE lead to larger rotors? This is not self-evident. A reference or elaboration would help. Similar on second sentence too relative mass to what? Refer to square cube law perhaps veers et al 2019 as well as the longer IEA Wind report dykes et al 2019 go into detail on this: <https://www.nrel.gov/docs/fy19osti/72437.pdf>. Sorry to be picky but as an opening to the paper, it should be stronger.

**Authors' response #3:** This is a very valuable remark. We have reformulated the introduction and added more references to this.

**++ detailed comment #3 ++ associate editor:** The uniqueness of the present work compared to Winthroth et al 2014 would be nice to call out explicitly directly after that work is cited. See overall comments, the novelty of this paper needs to be further espoused and built up if the use of a single 5 minute period of the measurement campaign (in results section) is to be justified.

**Authors' response #4:** This is a very important remark, thank you for

pointing this out. We changed the structure and formulation of the introduction part and further elaborated on the differences and novelties in comparison with the work that is already published.

**++ detailed comment #4 ++ associate editor:** Since the article at the beginning uses validation of aeroelastic codes as motivation for the work, it is underwhelming to simply report the solver being used without more details on the simulation setup. Though BHawC is a property code, minimum details about its physical modeling characteristics should be set up what type of aerodynamic solver, structural solver, etc? I believe you are using the statistics of the wind conditions of the site to produce the wind field that is fed to the solver but it is not very clear since there really isn't a good description overall of the experimental setup.

**Authors' response #5:** This is true, so we added more information on the solver and the simulations. Statistics of wind conditions were used for the simulations, which we emphasized more clearly.

**++ detailed comment #5 ++ associate editor:** I agree with the reviewer 2 comments on the turbulent seeds. It is very odd to show simulations from multiple turbulent seeds versus statistics. Even if you are simply trying to show the comparison, I would still show the simulation results with a mean and standard deviation or percentile band as that is common practice. The same recommendation goes for figures 21-24, the graphs are hard to read as it is and you could mitigate this simply by providing the mean across the simulations with a standard deviation band around it

**Authors' response #6:** We changed the plots according to your suggestion and completely agree with you, that the plots are much better to read now.

**++ detailed comment #6 ++ associate editor:** Psd is very interesting but it would be nice to see the analysis completed for more than one sample.

**Authors' response #7:** The PSD was updated to involve not only one simulation but the mean of all simulations.

## **2 List of changes**

### **2.1 Abstract**

- shortened and clarified the abstract

### **2.2 Introduction**

- elaborated on the context between reduced costs and the size of the rotor
- added more references to underline the statements
- further elaborated on the novelty of this paper in comparison with already published work
- introduced the use of a single five minutes measurement time series as an exemplary comparison between measurements and simulations

### **2.3 Experimental Setup**

- no changes made in this section

### **2.4 Digital Image Correlation**

- no changes made in this section

### **2.5 Determination of rotor blade deformation and torsion**

- no changes made in this section

### **2.6 Results**

- updated the description of aeroelastic code and the use of statistical wind conditions
- joined the single simulations of multiple turbulent seeds to one resulting curve with mean and standard deviation for all plots including simulation results

### **2.7 Conclusions**

- small changes in wording
- further elaborated on future work for the validation of aeroelastic codes based on more series of measurements

### **2.8 References**

- added more references for the introduction and for aeroelastic simulations

### 3 Revised manuscript



# Full scale deformation measurements of a wind turbine rotor in comparison with aeroelastic simulations

Stephanie Lehnhoff<sup>1</sup>, Alejandro Gómez González<sup>2</sup>, and Jörg R. Seume<sup>1</sup>

<sup>1</sup>ForWind, Institute of Turbomachinery and Fluid Dynamics - Leibniz Universität Hannover

<sup>2</sup>Siemens Gamesa Renewable Energy A/S

**Correspondence:** Stephanie Lehnhoff (lehnhoff@tfd.uni-hannover.de)

## Abstract.

The measurement of deformation and vibration of wind turbine rotor blades in field tests is a substantial part of the validation of aeroelastic codes. This becomes highly important ~~as the length of rotor blades increases with the growth in demand for wind power. The requirement for field validation of the aeroelastic behaviour of wind turbines increases with the scale of the deformation, in particular for modern blades with~~ for modern rotors, as the rotor size increases which comes along with structural changes, resulting in a very high flexibility and coupling between different vibration modes. However, performing ~~full-scale~~ full scale field measurements for rotor blade deformation is not trivial and requires high temporal and spatial resolution. A promising deformation measurement technique is based on an optical method called Digital Image Correlation (DIC). ~~A system for the application of DIC for full field measurements of wind turbine rotors has been developed and validated in the past years by ForWind, Institute of Turbomachinery and Fluid Dynamics, Leibniz Universität Hannover. The whole rotor of the wind turbine is monitored with a stereo camera system from the ground during measurement.~~ Recently, DIC measurements on a Siemens Gamesa SWT-4.0-130 test turbine were performed on the tip of all blades with in combination with marker tracking at the hub for the first time with synchronized measurement of the inflow conditions by a ground-based LiDAR. As the turbine was additionally equipped with strain gauges in the blade root of all blades, the DIC results can be directly compared to the actual prevailing loads to validate the measurement method. In the end, an example for a comparison of the measured deformations ~~are compared to aeroelastic simulations.~~

~~The deformation measured with DIC on the rotor blade tips shows the same qualitative behaviour when compared to loads measured with strain gauges in the blade root. This confirms that the DIC measurements correlate with the prevailing loads in reality. The comparison with aeroelastic simulations shows that the amplitude and trend of the in-plane deformation is in very good agreement with the DIC measurements. The out-of-plane deformation shows slight differences, which could be caused by the difference between real wind conditions and the wind statistics on which the simulations are based. The combined rotor blade pitch and torsion angle measured with DIC is in good agreement with the actual pitch value of the turbine. A detailed comparison with aeroelastic simulations shows that the amplitude of torsion measured with DIC is higher which might be caused by an inaccuracy of the experimental setup. This will be focus of future work.~~ and torsion with aeroelastic simulations is shown in the time and frequency domain. All in all, DIC shows very good agreement with comparative measurements and

simulations which shows that it is a suitable method for ~~measurements~~ measurement of deformation and torsion of multi-megawatt wind turbine rotor blades.

**Keywords.** full scale measurements, wind turbine rotor blade deformation, digital image correlation

## 1 Introduction

30 The increasing demand ~~in reduction of costs per kWh of wind turbines results in ever larger rotor diameters. In recent years, this~~  
~~has led to a crucial change~~ for a reduction of levelized costs of electricity (LCOE) of wind turbines leads to substantial changes  
in the design, operation, and reliability of wind turbines and plants (Dykes et al. (2019)). One leading driver for the reduction  
of LCOE for onshore turbines are changes in the design of the rotor: by increasing the rotor size (Wiser et al. (2016)). This  
is only possible by realizing crucial changes in the structural design of wind turbine blades, as the ~~relative~~ mass of the ~~blade~~  
35 ~~needs to decrease for a product to be economically viable. The~~ blades naturally scales with the volume and thus with the cube  
of the rotor blade length, whereas the energy capture scales only with the area of the rotor and thus with the square of the rotor  
blade length (the so-called "square-cube law"). The need for a reduction of mass per rotor blade length is realized by applying  
methods for the reduction of the volume, like aeroelastic tailoring. Thus, the knowledge of the aeroelastic behaviour is one of  
the biggest challenges in today's ~~wind turbine engineering~~ and especially in ~~the future~~ future wind turbine engineering (Veers  
40 et al. (2019)).

Along with this comes the need for experimental validation of aeroelastic modelling. Until today, the load of wind turbine  
rotor blades is usually measured with strain gauges in edgewise and flapwise directions, however measuring the rotor blade  
deformation and torsion is still a challenge. Optical measurement methods can make a contribution to this. In the past, several  
optical measurement methods were successfully applied on ~~full-scale~~ full scale wind turbines for the determination of rotor  
45 blade deflections during operation (Schmidt Paulsen et al. (2009), Ozbek and Rixen (2013), Grosse-Schwiep et al. (2014),  
Lutzmann et al. (2016)).

For the direct measurement of rotor blade deformation (in-plane as well as out-of-plane) and torsion of ~~full-scale~~ full scale  
wind turbines, only a few suitable measurement methods exist which are shortly introduced. In the past years, Siemens Gamesa  
developed an in-house photographic method for the detection of these variables (Mayda et al. (2013)). For this method, a  
50 camera is installed in the blade root region of a rotor blade, facing the blade tip. At different radial positions, optical markers  
are installed upright relative to the pressure side and on these sections, the deformation and twist can be detected. Another  
method called BladeVision was developed by SSB Wind Systems (Nidec SSB Wind Systems GmbH (2020)). For this method,  
a camera is installed in the inner side of the blade root region of the blade. Reflectors are also installed inside at different radial  
positions and are monitored by the camera for the determination of deformation and twist on those positions. Another method  
55 was developed by ForWind, Institute of Turbomachinery and Fluid Dynamics, Leibniz Universität Hannover. This method is  
based on Digital Image Correlation (DIC).

For this method, a stereo camera system is installed in the area in front of the turbine and ~~certain~~ random speckle patterns  
are applied on the blades' pressure side. On those sections where the pattern has been applied, the deformation and torsion of  
the rotor blade can be detected. All of the three optical methods described above have advantages and disadvantages. As an  
60 example, DIC is sensitive to the changing weather conditions outside, but it can be easily installed on the blade compared to  
the other two methods.

Before DIC was applied at full scale wind turbines, the feasibility and accuracy was determined on a scaled wind turbine model (Winstroth and Seume (2014a)) as well as within a fully virtual experiment (Winstroth and Seume (2014b)). Afterwards, the feasibility of this measurement method at full scale on a 3.2 MW wind turbine was proven (Winstroth and Seume (2015)).  
65 Wu et al. (2019) have demonstrated the applicability of the method by successfully applying DIC on a 5 kW wind turbine to obtain the full-field displacement and strain of the rotor blades. A comparison of out-of-plane deformations (measured with DIC) with aeroelastic simulations for a short time series of 30 seconds was also done (Winstroth et al. (2014)). The results show that such a comparison is not trivial, as the selection of time series can have a significant influence on the results ~~Regardless, these measurements are still a valid~~ when the time series is very short and the simulations are based on statistical  
70 wind conditions.

The next step is now the conduction of a longer time series and a comparison with high fidelity aeroelastic simulations, which includes both, deflections and torsion. This will be part of this paper in order to prove that DIC can be a beneficial tool for the validation of aeroelastic codes. All of the three methods described above have advantages and disadvantages. As an example, DIC is sensitive to the changing weather conditions outside, but it can be easily installed on the blade compared to  
75 Additionally, the other two methods.

~~This paper shows results~~ DIC results will be compared to load measurements in the frequency domain to validate this technique with conventional measurement methods. A five minute time series of DIC measurements on a wind turbine in the field and a comparison with aeroelastic simulations. will be used to show the feasibility and thus the potential of validating aeroelastic codes based on DIC measurements.

80 Firstly, the experimental setup for the execution of optical measurements on a full scale wind turbine is described. The speckles for DIC were applied in the tip region on all three blades. For the detection of the movement and rotation of the hub, three big speckles were applied on the hub itself. The hub movement is later on used for the determination of in-plane deformation (IP), out-of-plane deformation (OoP) and torsion out of the DIC signal. Afterwards, the functionality of the two optical methods applied, DIC and Marker Tracking, are briefly explained. Measurement results are shown and compared to  
85 strain gauge signals at the blade root for a qualitative experimental validation of the optical method. For a rough validation of the combined rotor blade pitch and torsion angle, the DIC signal will be compared to the pitch signal of the turbine. This can only prove a trend, as there is no additional measurement technique installed for the determination of rotor blade torsion. Results of a power spectral density estimation (PSD) with the Welch's method of the signals will be shown and compared to the natural eigenfrequencies that are expected to occur from numerical computations. Finally, the one time series of DIC  
90 measurements will be compared to aeroelastic simulations of the turbine ~~as a first try for an experimental validation of to~~ demonstrate a way of experimentally validating rotor blade deformation and torsion, based on DIC measurements.

## 2 Experimental Setup

The general measurement setup for the execution of DIC measurements on wind turbines is shown in Figure 1. Different radial positions of the blades can be equipped with self-adhesive foils to build a speckle pattern on the rotor blade. The deformation

95 can be captured in those areas where the speckles are applied, so this could be done along the whole length of the blade. A stereo camera system is placed in the area upstream of the turbine to monitor the whole rotor during operation.

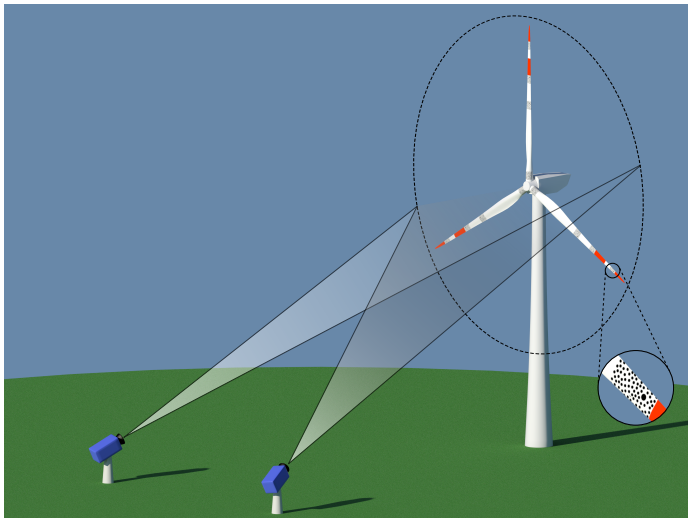


**Figure 1.** Schematic of a camera setup in front of a [full-scale](#) [full scale](#) wind turbine. The magnified cutout near the blade tip shows the random black-and-white pattern on the pressure side (Winstroth and Seume (2015)).

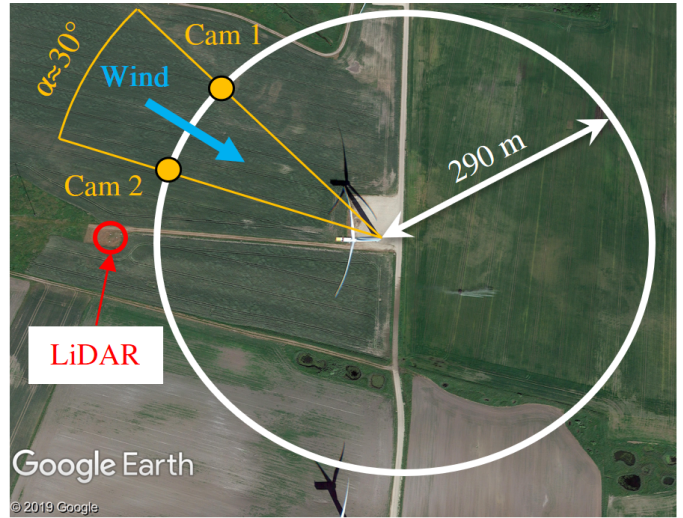


**Figure 2.** Experimental setup at the Høvsøre wind turbine test site.

In this measurement campaign, a Siemens Gamesa SWT-4.0-130 test turbine located at the DTU wind turbine test center in Høvsøre in Denmark, was equipped with a speckle pattern for DIC measurements in the tip region of all three blades. The cameras have a resolution of 25 MPx, and take pictures simultaneously with a frame rate of 30 fps. Each camera is connected via CameraLink to a measurement computer to store the pictures directly on the hard drive. Due to the high data rate of 750 MBps per camera, the maximum measurement duration with the current setup is limited to 10 minutes. Usually it is not the hard drive which limits the measurement duration, rather the change in weather and ambient lighting conditions.

Each camera is equipped with a lens of a 58 mm fixed focal length. In order to monitor the full rotor diameter of 130 m, the cameras are placed 290 m away from the foundation of the turbine, see Figure 2. The cameras are positioned in a 30° stereo angle configuration relative to the wind turbine. The wind direction should remain constant in the region between the two cameras to have an optimal angle of sight for both cameras. The turbine is allowed to yaw within this region, but if the angle between the rotor plane and the camera becomes too sharp, the speckles can not be identified well enough. The wind speed and direction at 10 different heights throughout the full extension of the rotor is measured at a sampling frequency of 1 Hz with a LiDAR located at a distance of 2.5 rotor diameters in front of the turbine in order to be able to assess shear and veer properly. Furthermore, the atmospheric temperature, pressure, and humidity are also logged to estimate the air density.

The speckles were applied on the pressure side of the blades from a lift in the range from 55 m to 60 m measured from the blade root, see Figure 3. The speckle pattern needs to be different for all blades, as DIC finds a unique greyscale signature for

every measurement point. Per blade, approximately 50 speckles with a diameter of 20  $\mu\text{m}$  were applied that build a random black-and-white speckle pattern. The hub is used to define the rotor plane and the rotational axis. In this case, three single dots with a diameter of 70  $\mu\text{m}$  were applied, which are analyzed with a Marker Tracking algorithm (see Figure 4).

The turbine is instrumented with strain gauges in the root of all three blades and furthermore, the following operational parameters are logged: pitch, rotor speed, and power with a 25 Hz sampling frequency. This is useful for a comparison of DIC with conventional measurement methods in the field.

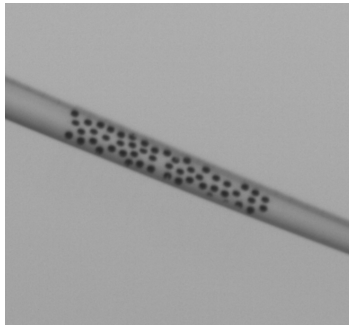


**Figure 3.** Random speckle pattern for the application of DIC on the blade tips.

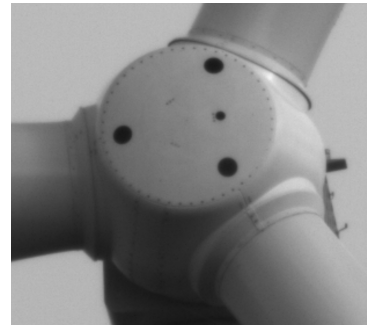


**Figure 4.** Three big dots on the nacelle for the application of Marker Tracking on the hub.

DIC is typically used in laboratory environments with constant illumination. As this setup is now applied in the field where the sun is the only suitable light source, a great deal of experience is required to perform a successful measurement under these conditions. The movement of clouds makes it a challenge to find a time slot which is longer than 5 minutes where illumination conditions remain constant.

The difference between DIC and Marker Tracking is that with Marker Tracking the single dots are tracked and not the full-field area between them. The advantage is that the position of the single markers is clearly defined, which comes along with the disadvantage of a higher inaccuracy. Out of this setup, the track of three single dots is extracted to define the rotor axis and the rotor plane. The blade tip regions are evaluated with the DIC algorithm and result in an areal information of the whole speckle pattern area, defined by the track of approximately 1000 points per blade tip.

### 3 Digital Image Correlation

In general, the term Digital Image Correlation describes an optical measurement method which is part of photogrammetry, that acquires images to calculate the full-field shape, deformation and/or motion measurements of certain objects (Sutton et al. (2009)). This process consists of the digital image acquisition itself, the storage and the performance of an image analysis to obtain motion and deformation out of the images. In this part, the analysis will be briefly described. The reader is referred to Sutton et al. (2009) for a more detailed description of the analysis methods.

The DIC algorithm applies several different analysis methods. It all starts with the recognition of the same points in all  
 135 images. This process is shown in Figure 5 for one measurement point.

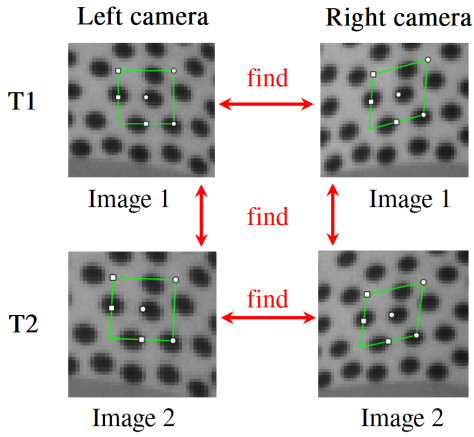


**Figure 5.** DIC algorithm finds points by tracking the greyscale signature of the subset in every picture.

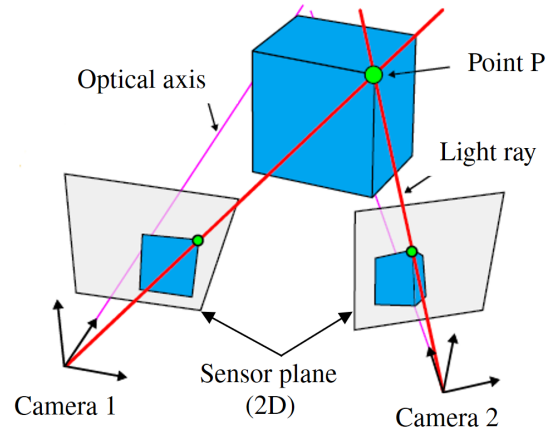


**Figure 6.** The position of the point P in 3D is calculated by the position of the two cameras relative to the wind turbine, and the individual position of the measurement point in the left and right picture.

The white dot in the middle of the green rectangle is the actual measurement point, which is defined by the greyscale signature  $F$  of the neighbouring pixels, that form a subset (green rectangle). The greyscale signature is defined as the distribution of greyscale values of all pixels in the defined subset and is a function of the local coordinates  $F = f(\mathbf{x})$ , where  $\mathbf{x}$  is defined as a two-dimensional vector  $\mathbf{x} = (x \ y)$ . At the time  $T1$ , the measurement point in image 1 of the left camera (usually the  
 140 reference picture), is defined and is found in the following pictures as the greyscale signature  $G$ , which is a function of the local coordinates and a displacement term  $\mathbf{p}$ , resulting in:  $G = f(\mathbf{x}, \mathbf{p})$ . The greyscale value of a certain subset is obtained by building the sum of greyscale values of all neighboured pixels in the subset in the form of  $\sum F$  and  $\sum G$ .

The reference subset is defined in the reference image 1 of the left camera and is usually rectangular. To find a similar (or  
 145 in perfect case the same) greyscale in the following pictures of the same camera, a shape function needs to be introduced, as the subset might not have the same shape. This shape function  $\xi(\mathbf{x}, \mathbf{p})$  is used to transform pixel coordinates in the reference subset into coordinates in the image after deformation. This results in a correlation function  $\chi$  that is dependent on the shape of the subset as follows:

$$\chi^2(\mathbf{p}) = \sum (G(\xi(\mathbf{x}, \mathbf{p})) - F(\mathbf{x}))^2. \quad (1)$$

The search for the best match between  $F$  and  $G$  is driven by computing the value of  $\chi$ , by iteratively updating  $p$ . For an  
150 affine transformation,  $\xi$  can be defined as:

$$\xi(\mathbf{x}, \mathbf{p}) = \begin{bmatrix} p_0 \\ p_1 \end{bmatrix} + \begin{bmatrix} 1 + p_2 & p_3 \\ p_4 & 1 + p_5 \end{bmatrix} \mathbf{x}, \quad (2)$$

where six components of  $\mathbf{p}$  are introduced.  $p_0$  and  $p_1$  define the translational displacement of the subset in the picture, whereas  $p_2, p_3, p_4$  and  $p_5$  change the rotation, compression and shear of the subset shape.

Different solving algorithms exist to find the optimal value of  $\chi$ , where for DIC, all are based on the normalized cross-  
155 correlation (NCC) criterion  $\chi_{NCC}^2$ , that is actually the origin of the term *correlation* in DIC:

$$\chi_{NCC}^2 = \frac{\sum FG}{\sqrt{\sum F^2 \sum G^2}}. \quad (3)$$

The correlation criterion  $\chi$  is bounded in the interval  $[0, 1]$ , where 1 represents the perfect match. Usually, the maximum match is found under application of the Levenberg-Marquardt algorithm (Levenberg (1944), Marquardt (1963)).

This criterion is extended to account for lighting offsets and scales relative to the reference picture, and results in the ero-  
160 mean normalized sum of squared difference (ZNSSD) criterion  $\chi_{ZNSSD}^2$ :

$$\chi_{ZNSSD}^2 = \sum \left( \left( \frac{\sum \bar{F}_i \bar{G}_i}{\sum \bar{G}_i^2} G_i - \bar{G} \frac{\sum \bar{F}_i \bar{G}_i}{\sum \bar{G}_i^2} \right) - F_i + \bar{F} \right)^2. \quad (4)$$

$\bar{F}_i$  and  $\bar{G}_i$  are defined as the difference of the current value to the mean value, resulting in  $\bar{F}_i = F_i - \bar{F}$  and  $\bar{G}_i = G_i - \bar{G}$ .

The stereo matching between the left and the right camera is done under application of a plane-to-plane homography matrix. This homography matrix relates image coordinates to coordinates on a plane in space. As the coordinates of both cameras in  
165 the world is known after the external calibration, image coordinates of the left camera can be related to image coordinates of the right camera through a homographic transformation, more commonly referred to as rectification in computer vision.

To achieve the maximum geometrical resolution, sub-pixel interpolation is applied in the matching algorithm. The sub-pixels are interpolated by a continuous 8-tap spline.

The result of the application of the DIC algorithm with the software Vic3D by Correlated Solutions, Inc. (Correlated Solu-  
170 tions, Inc. (2020)) can be seen in Figure 7. The measurement points that are obtained are highlighted in green. It can be seen that the algorithm did not converge in the outer region, which is due to the definition of the subset size.

This data set can be directly imported in Matlab, the result of which is shown in Figure 8. The measurement points are not aligned to the rotor coordinate system at this evaluation step.

The Marker Tracking algorithm also applies a sub-pixel interpolation to find the right match of the marker in all images,  
175 however there is no definition of subsets, as the marker itself is directly tracked. This guarantees that the exact position of the markers will be calculated, but results in a less accurate signal compared to the areal DIC method. This requires the application



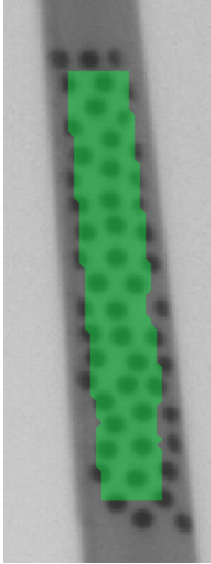


**Figure 7.** Measurement points plotted on the rotor blade

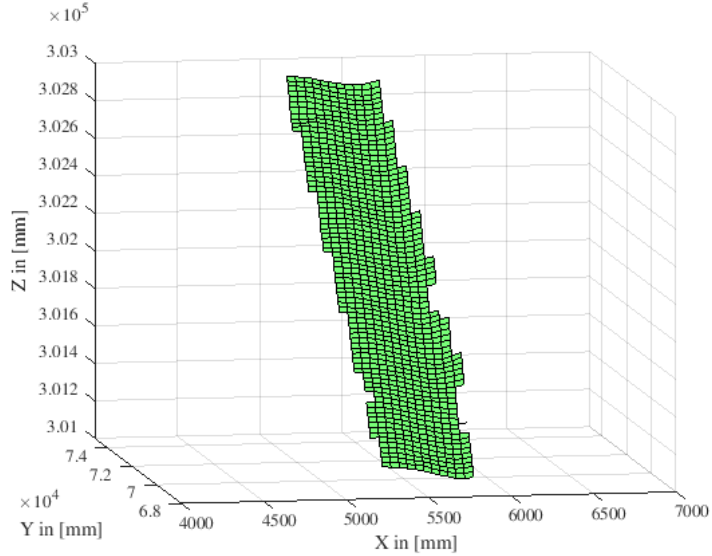


**Figure 8.** Measurement points plotted in 3D, not aligned to the rotor coordinate system

of a low pass filter to the hub track. As the movement of the nacelle is slow compared to the movement of the blade tips, this method is still suitable for the detection of the hub track. The areal DIC tracks are not filtered and thus can be used directly for evaluation.

#### 180 4 Determination of rotor blade deformation and torsion

The evaluation of the optical measurement is split into five main parts, which is shown in Figure 9. The first part **(1)** is the detection of the positions of the speckle pattern out of the pictures, i.e. the application of a DIC algorithm to the image series. This is done with the commercial software Vic3D from Correlated Solutions, Inc (Correlated Solutions, Inc. (2020)). The software can track the position of the speckle regions even under a rotating movement of the object. In a second step **(2)**, the movement of the hub is determined by tracking the position of the three markers on the hub itself with a Marker Tracking algorithm, which is also included in Vic3D. This defines the rotor axis as well as the rotor plane **(3)**, which is necessary for the next step. In a fourth step **(4)**, the positions are classified into in-plane deformation (IP) and out-of-plane deformation (OoP) by removing the hub movement from DIC data. The OoP deformation can be further used to calculate the torsional deformation of the rotor blade **(5)**.

190 The output of DIC is a full-field information of the position of the surface of the rotor blades' pressure side in 3D. An example for the direct output of one DIC measurement point is shown in Figure 10. The coordinate system is not aligned, thus the measurement point rotates around an undefined rotational axis. A change in the yaw position of the rotor can be clearly

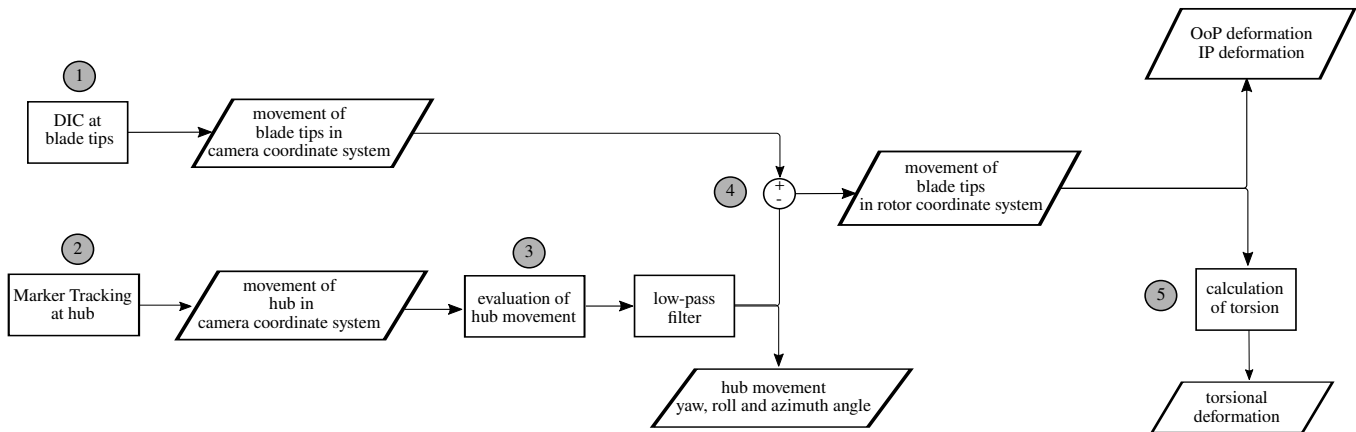


**Figure 9.** Evaluation of DIC and Point Tracking method for determination of rotor blade deformation and torsion

seen in this track. To define the deformation in OoP and IP, the rotor plane needs to be aligned with the rotor coordinate system. To define the position and orientation of the rotational axis, which is step (3), the tracks of the markers on the hub are used.

195 This is done in three steps:

- i) Translational alignment of the hub center to the origin of the coordinate system  
→ elimination of translational movement
- ii) Rotational alignment of the normal vector on the hub to the x-axis of the coordinate system  
→ elimination of yaw and roll angle
- 200 iii) Rotational alignment of the measurement point around the rotational axis  
→ elimination of azimuth angle

The translational displacement (i) of the rotational axis is found by determining the center of the position of the three markers. The markers are not perfectly positioned at the same distance to the rotational axis, which results in a remaining rotational radius of approximately 20 mm, which can safely be considered negligible. The translational displacement of the rotational axis is determined for every time step and removed from the original DIC data.

205 The rotational misalignment (ii) between the normal vector of the rotor plane and the x-axis in the coordinate system is determined. This results in two angles which are removed from the DIC data for every time step: yaw and roll angle. The result of this can be seen in Figure 11. What remains is the rotation around the x-axis, which is defined as the azimuth angle.

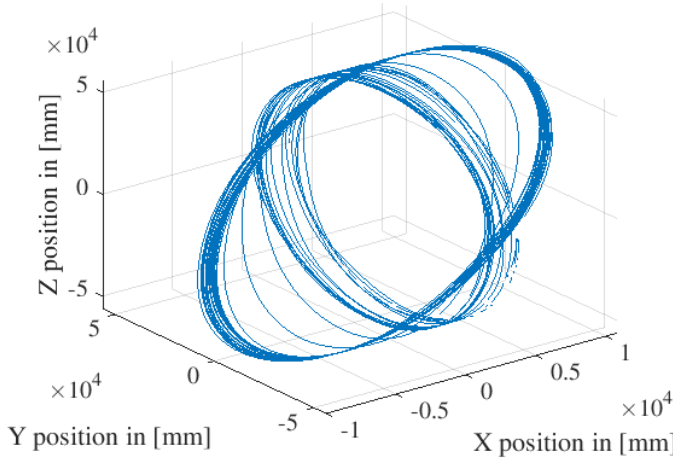


**Figure 10.** Track of one measurement point of DIC without alignment

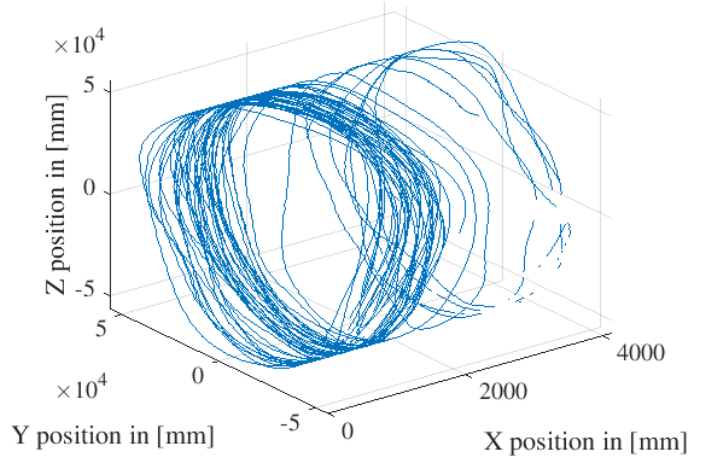


**Figure 11.** Track of one measurement point of DIC aligned to the rotor plane

In a third step, the azimuth angle needs to be removed (iii). For this, the reference measurement point of the center of rotation is aligned with the z-axis. The azimuth angle is determined as the rotational offset around the x-axis between the actual measurement point and the reference point. Now that the azimuth-angle is determined, it can be removed from the DIC signal that is aligned with the rotor plane.

The displacement that remains in the DIC measurement points is defined as follows:

- movement in x-direction → out-of-plane deformation (OoP)
- movement in y-direction → in-plane deformation (IP)
- movement in z-direction → radial deformation

The radial deformation is affected by the radial displacement of the hub marker center to the actual rotational axis remaining in the measurement data.

Figure 12 shows a view of the rotor blade chord of length  $c$  in relative position to the rotor plane. The angle  $\beta$  defines the rotation around the vertical axis of the rotor blade, and is a combination of pitch and torsion angle. This angle can be determined by the position of points between the leading edge  $P_{LE}$  and the trailing edge  $P_{TE}$ :

$$\beta = \arcsin \left( \frac{x(P_{TE}) - x(P_{LE})}{c} \right) = \arcsin \left( \frac{dx}{c} \right). \quad (5)$$

Depending on the value of  $c$ , the resolution of the OoP position may need to be very accurate to determine the torsion angle. If  $c$  has a value of 700 mm and  $\beta$  should be determined with a resolution of  $0.1^\circ$ , then  $dx$  needs to be resolved with an accuracy of 1.2 mm.

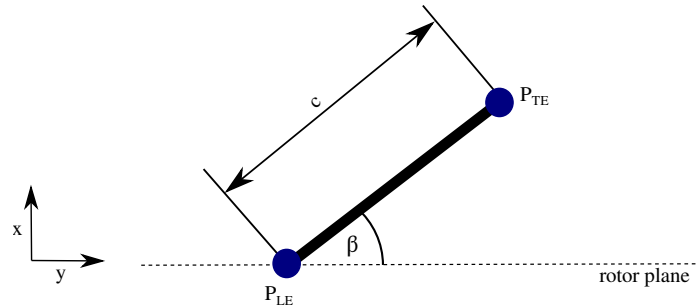


**Figure 12.** Determination of the pitch + torsion angle  $\beta$  out of DIC measurements;  $c$ : chord length of the rotor blade,  $x$ : OoP position,  $y$ : IP position

## 5 Results

This section contains measurement results of one DIC measurement time series and related simulations. The DIC measurement duration was five minutes and the simulations were ~~done-conducted~~ for a ten minute time series, ~~reproduced by the mean based on the statistics of the~~ wind conditions during the ~~corresponding~~ time slot. For the simulations, the aeroelastic solver  
 230 BHawC (Siemens Gamesa in-house aeroelastic solver (Rubak and Petersen (2005), Skjoldan (2011))) is used. ~~BHawC has been used for almost 15 years for the simulation of loads of both onshore as well as offshore wind turbines. The structural model of the solver is based on the non-linear Timoshenko finite element beam model based on a co-rotational formulation (Couturier and Skjoldan (2018)). The structural model is coupled with a standard Blade Element Momentum (BEM) code including a Beddoes-Leishman based dynamic stall model, a second-order dynamic inflow model, a standard Prandtl tip-loss~~  
 235 ~~correction, as well as a Glauert-type yaw-misalignment correction and an empirical correction for heavy loaded rotors .~~

The aeroelastic simulations are carried out in a so-called one-to-one fashion (see Enevoldsen (2014)). The structural model is matched exactly to the particular turbine in geometry and structural description. In addition to this, the system dynamics are represented in high resolution, as the atmospheric inflow conditions are recreated numerically according to the statistics of the wind corresponding to that exact time series. Several turbulence boxes were generated for these conditions, all of them  
 240 with the same statistics, with the aim of reducing the uncertainty. The wind field is modelled as accurately as possible with the available instrumentation and statistics collected, but a full wind field recreation based on time-series measurements is not available. Usually, a minimum of six and a maximum of 20 simulations with the same ~~mean-statistical~~ wind conditions, but under variation of turbulence seeds, are conducted for a time series. In this case, nine simulations were conducted to become independent of the influence of turbulent seeds.

245 The ~~mean-statistics of the~~ measured wind conditions during the time period are shown in Table 1. These conditions were measured by the ground-based LiDAR ~~upwind of the turbine (see Section 2)~~. The azimuth angle in the following diagrams is defined according to Figure 13. From the DIC measurements, a point was chosen which is placed on a radial position of 56.5 m, and the numerical model was setup to have an output point at the same radial position. Therefore, all following results for

measurements and simulations were extracted at a radial distance of approximately 56.5 m distance to the blade root.

250

**Table 1.** Statistics of measured wind conditions as input for simulations

Property	Value
Air density	1.226 kg/m <sup>3</sup>
Wind speed	16.48 m/s
Average yaw error	-4.28°
Turbulence intensity	0.0693 %
Average shear coefficient	0.078 65
Simulation duration	600 s

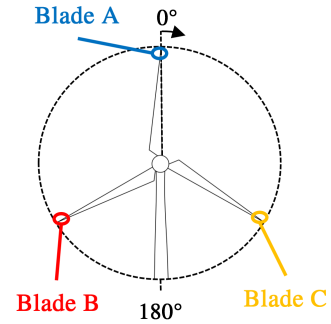


**Figure 13.** Definition of azimuth angle

### 5.1 Rotor blade deformation

Figures 14 to 17 show the output of processed DIC measurements on all blades. In the OoP time series the influence of a continuous change in pitch angle can be clearly seen. At the beginning of Figure 15, an asymmetric flapwise vibrational behaviour can be seen on all rotor blades for a few seconds. A direct comparison of OoP and IP deformation shows that the amplitude of IP deformation is higher compared to OoP.

255

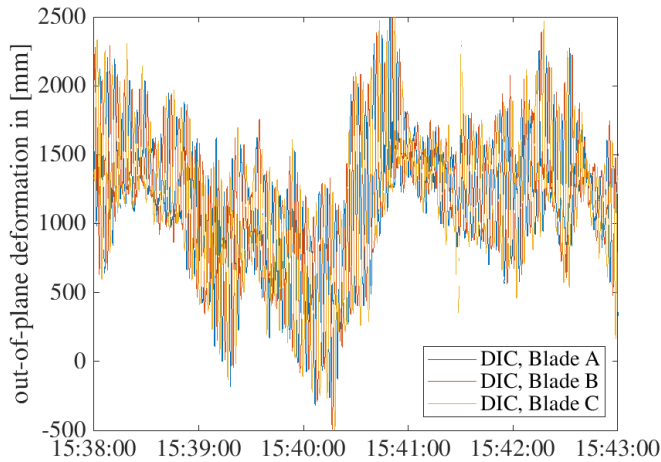


**Figure 14.** OoP DIC signal of all blades

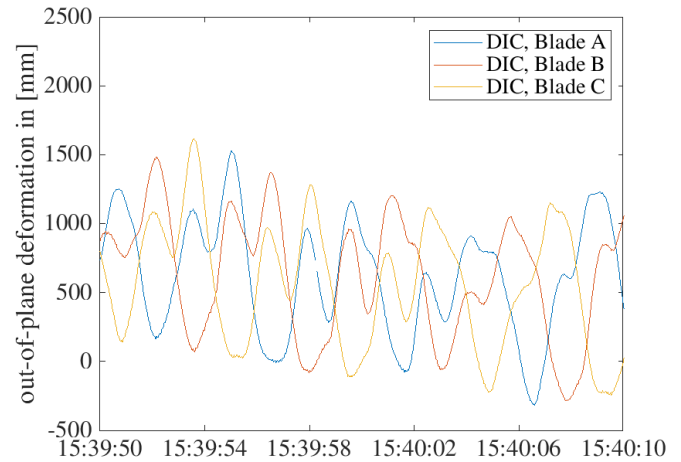


**Figure 15.** OoP DIC signal of all blades - Zoom

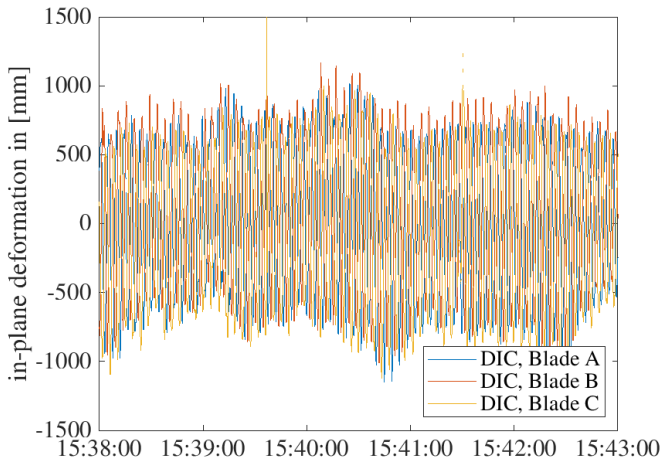


**Figure 16.** IP DIC signal of all blades

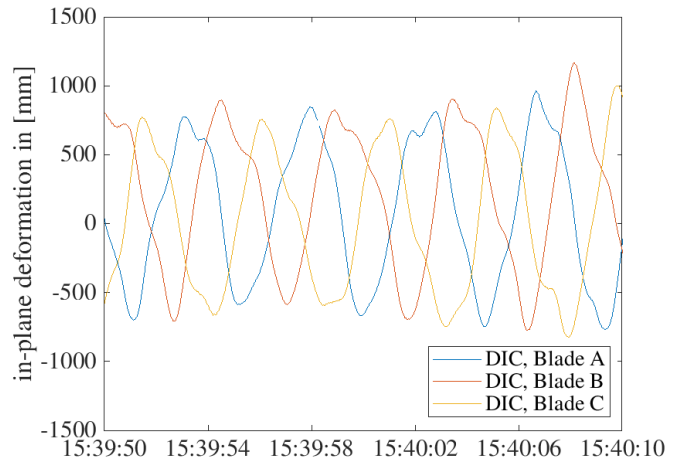


**Figure 17.** IP DIC signal of all blades - Zoom

Figure 18 shows a qualitative comparison of the flapwise bending moment in the blade root and the deformation at the blade tip in OoP direction.

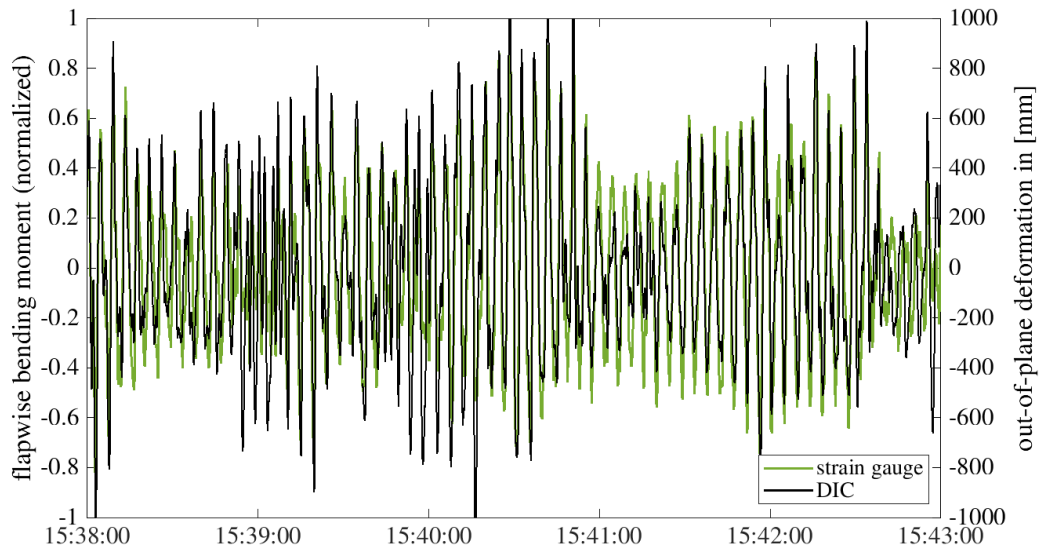


**Figure 18.** Qualitative comparison of measured flapwise bending moment and OoP deformation of Blade B

Both variables have been reduced by their moving average for an improved comparability. It can be seen that the qualitative behaviour of both variables is nearly identical which confirms that the OoP deformation of rotor blades, measured with DIC, corresponds to the flapwise loads prevailing in reality. The same behaviour can be ~~shown~~observed for IP deformation in com-

parison with the edgewise bending moment.

### Comparison with aeroelastic simulations

265

In ~~Figure~~ Figures 19 and 20, a cut-out of OoP and IP deformation of Blade B measured with DIC is shown in direct comparison with simulation results ~~-over time~~. The simulation results are presented as the mean and standard deviation of all nine simulations that were conducted. At first sight, the OoP DIC signal ~~is in good agreement with the simulations~~ shows differences in the position of the minimum and maximum deformation, while the IP DIC signal ~~shows a slightly lower amplitude compared to single~~ is in very good agreement with the simulations.

270

~~Comparison of OoP deformation measurement and simulations of Blade B- short time series~~ Comparison of IP deformation measurement and simulations of Blade B- short time series

For a better comparison over the whole time series, the deformation is plotted against the azimuth angle. ~~In~~ Figures 21 and ??-22 show the mean results for OoP and IP deformation against azimuth angle ~~are shown~~. The simulation results are again summarized to obtain mean and standard deviation values. The values are divided into 1° bins of azimuth angle and the values for the corresponding mean value and standard deviation are obtained.

275

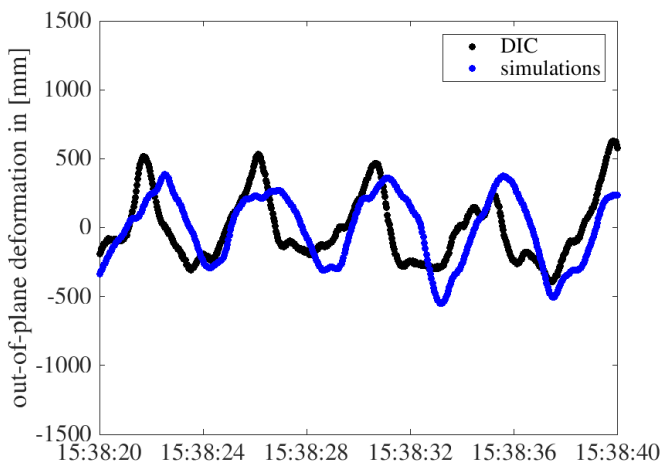


**Figure 19.** Comparison of OoP deformation measurement and simulations of Blade B- short time series

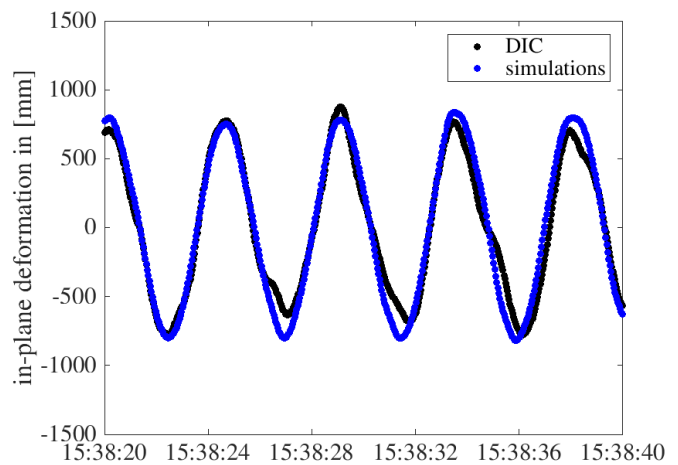


**Figure 20.** Comparison of IP deformation measurement and simulations of Blade B- short time series

In general, the OoP deformation measured with DIC is in ~~very~~ very good agreement with the simulations. ~~The maximum~~ Overall, the simulations and measurements overlap always within the band of standard deviation and the maximum and minimum amplitude have a similar value. However, the maximum OoP deformation for simulations of Blade B appears at approximately 180°, while for DIC it is shifted and appears at around 250°. One reason for this could be an influence of the actual prevailing weather conditions. The simulations are based on statistics of the wind measurements of ten minutes, while the measurements

280

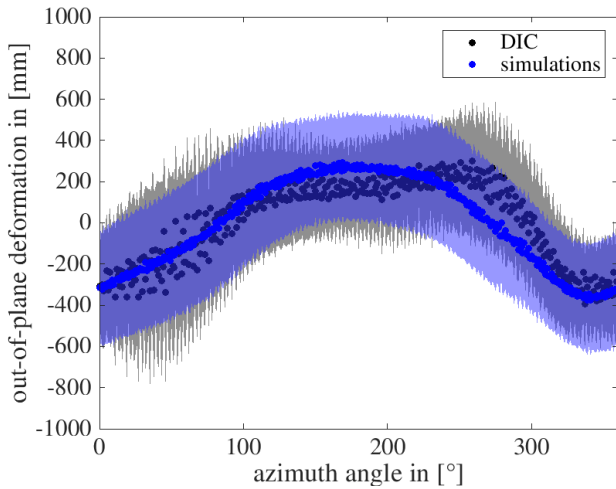


**Figure 21.** Comparison of OoP deformation of DIC and simulations of Blade B - mean values with standard deviation

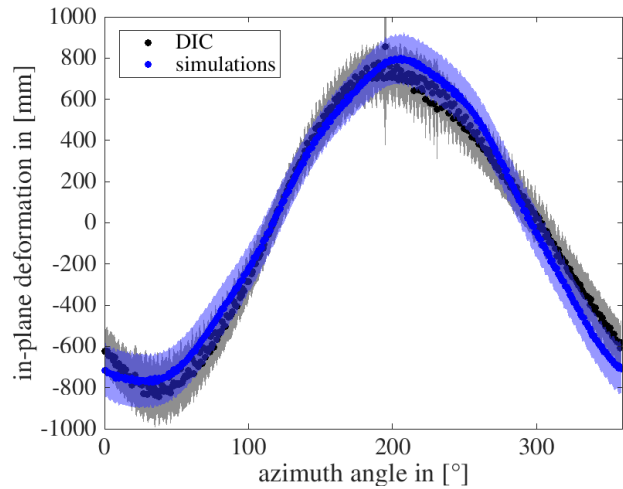


**Figure 22.** Comparison of  $\Theta_{\text{IP}}$  deformation of DIC and ~~simulation no. 1 simulations~~ of Blade B - mean values with standard deviation

are a result of the real wind conditions which can be different in this case. ~~The standard deviation for both simulations and DIC are in good agreement, as can be seen in Figure ??.~~

285 The IP deformation of DIC is in very good agreement with the simulations, which is shown in ~~Figures 22 and ??~~ Figure 22. The location of minimum and maximum IP deformation is nearly the same and so is the amplitude and the related standard deviation.

~~Comparison of IP deformation of DIC and simulation no. 1 of Blade B -- whole time-series Comparison of IP deformation of DIC and simulations of Blade B -- whole time-series~~

## 5.2 Rotor blade torsion

290 A result for the combination of rotor blade pitch and torsion angle measured with DIC is shown in Figure 23. The DIC signal follows clearly the pitch signal of the turbine for all three blades. In comparison with results from simulation no. 1, as shown in Figure 24, the amplitude of measured torsion is higher. In reality, the pitch signal has a higher range (from 17° to 11°) compared to simulation no. 1 (from 14° to 11°), but this can not explain the difference between measured and simulated torsion.

295 A direct comparison between measured and simulated torsion is shown in Figure 25. The moving average has been removed from all data sets and shows clearly, that the torsion measured with DIC is higher compared to simulations, but generally shows the same trend. This becomes even clearer when the torsion is plotted against deformation, as shown in Figure 26. The trend of the coupling between rotor blade torsion and OoP deformation can be reproduced from the DIC measurements, but with a significantly higher amplitude.



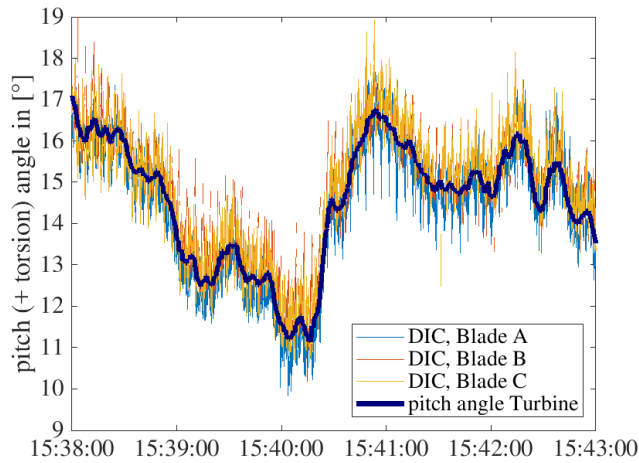


**Figure 23.** Masured wind turbine pitch angle and DIC Pitch + Torsion angle

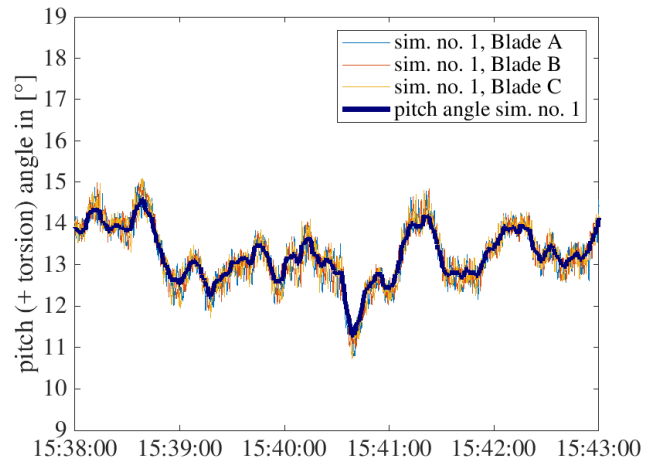


**Figure 24.** Simulated Pitch + Torsion angle of simulation no. 1 of all blades

300 The reason for this difference could lie either in an inaccuracy of the simulation or of the DIC measurement. However, if the torsion would have an amplitude as high as that measured with DIC, the actual measured loads would be expected to give significantly different values, too. As this is not the case, the dynamic amplitude of torsion measured with DIC is physically not plausible in this case. The reason for this is not clearly identified by now and will be further investigated. As it is known from past measurement campaigns, the spatial resolution and thus the accuracy of DIC can be improved by increasing the number of speckles on the blades, ~~what~~which will be taken into account for future measurement campaigns.

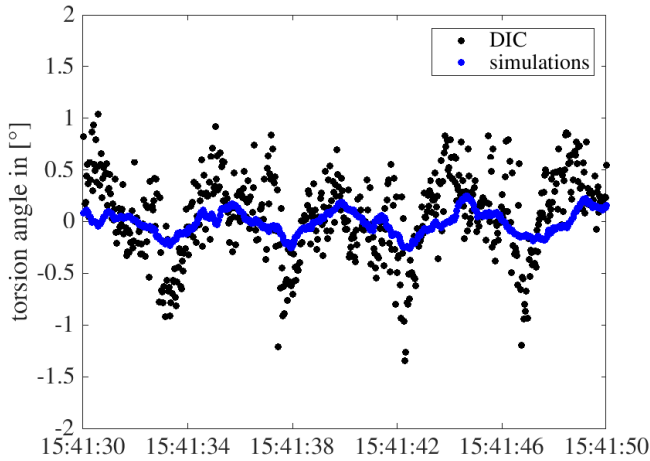


**Figure 25.** Comparison of torsion angle of Blade A of DIC and simulations - short time series

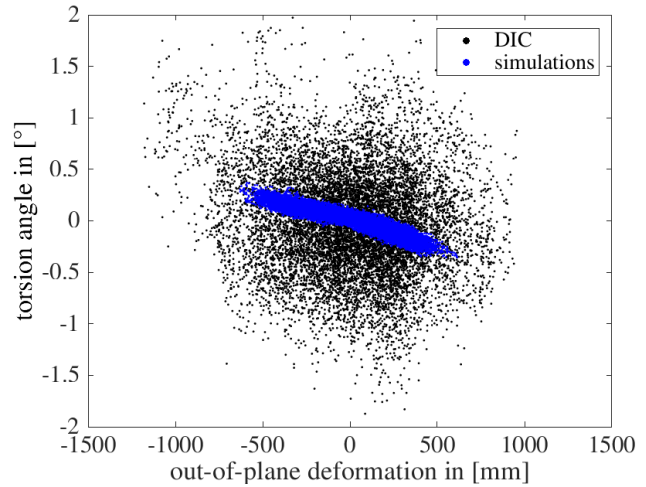


**Figure 26.** Coupling of rotor blade torsion and OoP deformation

### 305 5.3 PSD

Lastly, deformations measured with DIC are compared to simulations and bending moments in the frequency spectrum obtained with the Welch's method. Figure 27 shows the frequency spectrum of the flapwise bending moment and the OoP deformation. The signal of strain gauges in the blade root from measurement and ~~simulation no. 1~~ simulations are overall in good agreement. The measurement shows clear peaks at 1P and its ~~multiples~~ multiples, whereas the ~~simulation shows in the 2P range~~ simulations show a number of smaller peaks in the 2P range. For the OoP deformation, the PSD of the DIC signal is in good agreement with ~~simulation no. 1~~ the simulations. The main peaks ~~occur~~ occur at 1P and its multiples. Right behind the 2P frequency, a small peak can be observed which belongs to the frequency of the first flapwise mode.

The PSD of edgewise bending moment and IP deformation is shown in Figure 28. The signal of strain gauges in the blade root from measurement and ~~simulation no. 1~~ simulations are in good agreement. This proves that the simulated loads are close to the real loads in this time series. The first edgewise mode between 3P and 4P can be clearly identified out of both signals. The same peak can be observed in the PSD curves of the IP deformation measurement and ~~simulations~~ simulations. Furthermore, the IP deformation measurement shows a peak ~~in the region of the~~ right behind the 2P frequency, which belongs to the first flapwise mode. A small peak at the frequency of the second flapwise mode can only be seen in the PSD of the simulated flapwise bending and IP deformation. A reason, why this is not seen in the DIC signal, could be, that the radial measurement position is not exactly the same in simulation and measurement and that the DIC measurement point is closer to the node of the second flapwise mode, so that the amplitude is too small to be clearly observed.

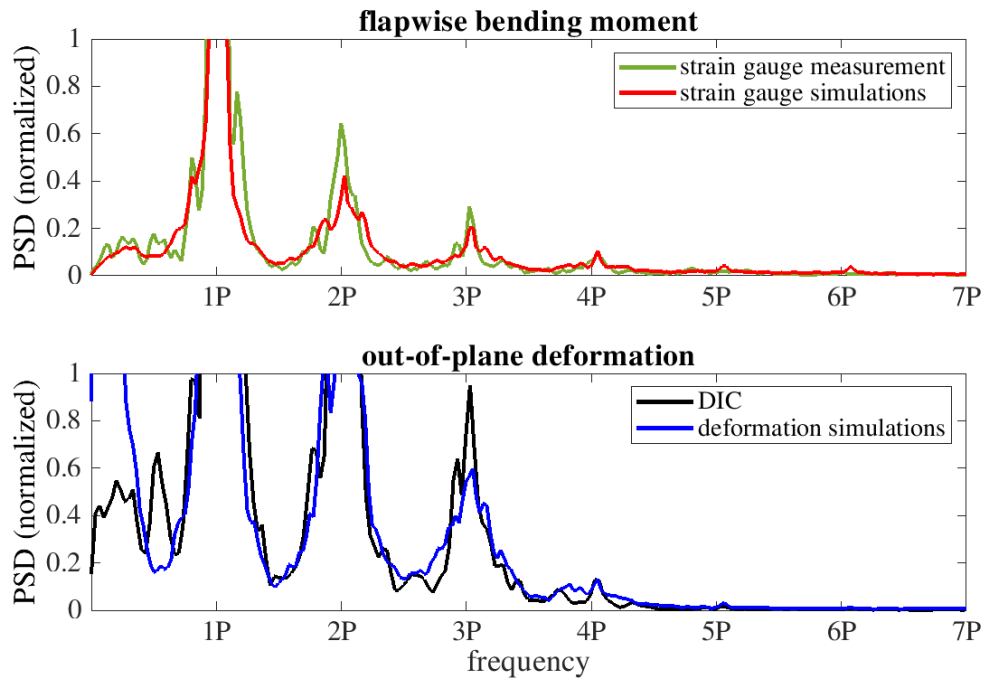


Figure 27. Comparison of PSD extracted with the Welch’s method for flapwise/OoP signals of Blade B

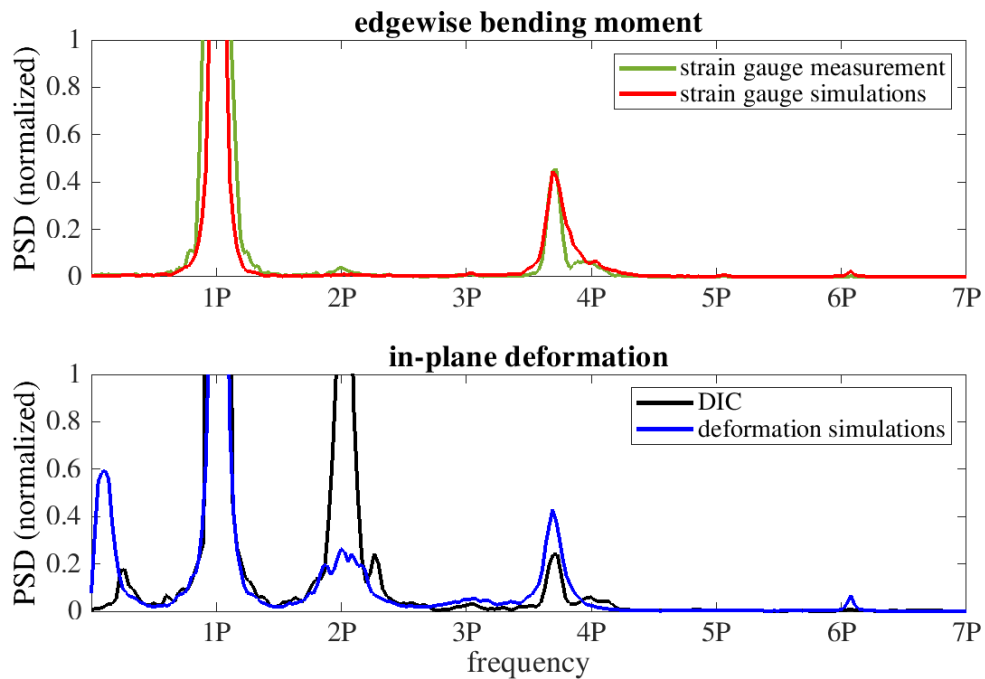


Figure 28. Comparison of PSD extracted with the Welch’s method for edgewise/IP signals of Blade B

## 6 Conclusions

This paper summarizes shortly the functionality of DIC and the application of this innovative measurement technique to ~~full-scale~~ full scale wind turbines. Furthermore, typical measurement results are shown and a comparison with measured root bending moments and simulations is evaluated.

The results show that rotor blade deformations measured with DIC qualitatively show the same trend when compared to strain gauges in the blade root for both OoP and IP. A direct comparison of measured and simulated deformations shows that both are in very good agreement. Small deviations can be seen, especially for OoP deflections. Those deviations can occur from the statistical character of ~~simulations~~ the simulations, which are hard to meet with a five minute measurement. The simulations are based on the mean wind conditions of ~~a ten minutes time series~~ the same time slot, which can cause a difference between simulated loads and reality. A direct comparison of a short time series of deformation measurements with statistical simulations remains a challenge. But still the results of this paper prove that DIC is a suitable method for the validation of rotor blade deformation at full scale.

The measurement of rotor blade pitch and torsion angle with DIC in this setup clearly follows the actual pitch angle of the turbine, which validates the method on average. However, the amplitude of the dynamic torsion is higher compared to simulations. This amplitude is physically not plausible, as the expected loads of the turbine would then be different, too. The reason for this is not clear yet and will be further investigated. One approach could be to improve the experimental setup, as the present one can be considered as minimalistic in that there were only 50 speckles applied on every blade. If the size of the speckles is reduced, the number of speckles on the blades can be increased which would come along with an improved spatial resolution of the rotor. This will be taken into account for future DIC measurements.

In summary, DIC can be considered a suitable method to measure rotor blade deformation and torsion and to validate aeroelastic simulations. ~~The method~~ It can be easily applied on rotor blades, even if the ~~rotor~~ blades are already installed on the turbine. In future work, the measurement accuracy for the rotor blade torsion will be improved by optimizing the experimental setup, in particular the speckle pattern on the blades ~~and on the hub~~, as well as the measurement equipment. Furthermore, a more detailed analysis based on a whole series of measurements will be conducted to perform a validation of aeroelastic codes with this short-term measurement technique. For this, SpinnerLidar data will be used to optimize the reconstruction of the wind field for simulations. DIC has a great potential for the experimental validation of the simulations of rotor blade deformation and torsion of wind turbines.

*Competing interests.* The authors declare that they have no conflict of interest.

*Acknowledgements.* ~~The authors~~ The authors gratefully acknowledge the financial funding from the Ministry of Science and Culture of Lower Saxony, Germany. The presented work was conducted in cooperation with the Collaborative Research Center 871 funded by the Deutsche Forschungsgemeinschaft (DFG, German Research Foundation) – SFB 871/3 – 119193472. We thank our colleagues at Siemens Gamesa and

TFD for the valuable discussions concerning the results of this work. We also thank the technical staff from Siemens Gamesa and TFD for their support during the measurement campaign.

## 355 References

- Correlated Solutions, Inc.: Deformation Measurement Solutions, Brochure, <https://www.correlatedsolutions.com/wp-content/uploads/2013/10/Vic-3D-Brochure.pdf>, 2020.
- Couturier, P. and Skjoldan, P.: Implementation of an advanced beam model in BHawC, *Journal of Physics: Conference Series*, 1037, 062 015, <https://doi.org/10.1088/1742-6596/1037/6/062015>, 2018.
- 360 Dykes, K., Veers, P., Lantz, E., Holttinen, H., Carlson, O., Tuohy, A., Sempreviva, A. M., Clifton, A., Rodrigo, J. S., Berry, D., Laird, D., Carron, S., Moriarty, P., Marquis, M., Meneveau, C., Peinke, J., Paquette, J., Johnson, N., Pao, L., Fleming, P., Bottasso, C., Lehtomaki, V., Robertson, A., Muskulus, M., Manwell, J., Tande, J. O., Sethuraman, L., Roberts, O., and Fields, J.: Results of IEA Wind TCP Workshop on a Grand Vision for Wind Energy Technology, Tech. rep., IEA Wind TCP, 2019.
- Enevoldsen, P. B.: Load validation and advanced modeling, *Advances in Rotor Blades for Wind Turbines*, IQPC Conference, Bremen, Germany, 2014.
- 365 Grosse-Schwiep, M., Piechel, J., and Luhmann, T.: Measurement of Rotor Blade Deformations of Wind Energy Converters with Laser Scanners, *Journal of Physics: Conference Series*, 524 012067, 2014.
- Levenberg, K.: A method for the solution of certain non-linear problems in least squares, *Quarterly of Applied Mathematics*, vol. 2, No. 2 (JULY, 1944), pp. 164-168, 1944.
- 370 Lutzmann, P., Goehler, B., Scherer-Kloeckling, C., Scherer-Negenborn, N., Brunner, S., van Putten, F., and Hill, C. A.: Laser Doppler Vibrometry on Rotating Wind Turbine Blades, 18th Coherent Laser Radar Conference, boulder, Colorado, USA, 2016.
- Marquardt, D. W.: An Algorithm for Least-Squares Estimation of Nonlinear Parameters, *Journal of the Society for Industrial and Applied Mathematics*, 11(2), 431–441, 1963.
- Mayda, E., Obrecht, J., Dixon, K., Zamora, A., Mailly, L., Sievers, R., and Singh, M.: Wind Turbine Rotor R&D - An OEM Perspective, 375 *International Conference on Future Technologies for Wind Energy*, october 7-9, 2013.
- Nidec SSB Wind Systems GmbH: More than a well-rounded solution: BladeVision, Brochure, [https://www.ssbwindsystems.de/pdf/SSB\\_Wind\\_Broschuere\\_BladeVision\\_EN.pdf](https://www.ssbwindsystems.de/pdf/SSB_Wind_Broschuere_BladeVision_EN.pdf), 2020.
- Ozbek, M. and Rixen, D. J.: Operational Modal Analysis of a 2.5 MW Wind Turbine using Optical Measurement Techniques and Strain Gauges, *Wind Energy*, vol. 16, No. 3, pp. 367-381, 2013.
- 380 Rubak, R. and Petersen, J. T.: Monopile as Part of Aeroelastic Wind Turbine Simulation Code, *Proceedings of Copenhagen Offshore Wind*, 2005.
- Schmidt Paulsen, U., Erne, O., Möller, T., Sanow, G., and Schmidt, T.: Wind Turbine Operational and Emergency Stop Measurements Using Point Tracking Videogrammetry, *Proceedings of the 2009 SEM Annual Conference & Exposition on Experimental & Applied Mechanics*, 2009.
- 385 Skjoldan, P.: Aeroelastic modal dynamics of wind turbines including anisotropic effects, PhD Thesis. DTU Risoe-PhD-66, 2011.
- Sutton, M. A., Orteu, J. J., and Schreier, H.: *Image Correlation for Shape, Motion and Deformation Measurements: Basic Concepts, Theory and Applications*, Springer US, iISBN 978-0-387-78747-3, 2009.
- Veers, P., Dykes, K., Lantz, E., Barth, S., Bottasso, C. L., Carlson, O., Clifton, A., Green, J., Green, P., Holttinen, H., Laird, D., Lehtomäki, V., Lundquist, J. K., Manwell, J., Marquis, M., Meneveau, C., Moriarty, P., Munduate, X., Muskulus, M., Naughton, J., Pao, L., Paquette, 390 J., Peinke, J., Robertson, A., Sanz Rodrigo, J., Sempreviva, A. M., Smith, J. C., Tuohy, A., and Wisser, R.: Grand challenges in the science of wind energy, *Science*, 366, <https://doi.org/10.1126/science.aau2027>, <https://science.sciencemag.org/content/366/6464/eaau2027>, 2019.

- Winstroth, J. and Seume, J. R.: Wind Turbine Rotor Blade Monitoring Using Digital Image Correlation: Assessment on a Scaled Model, 32nd ASME Wind Energy Symposium, 13-17 January 2014, National Harbor, Maryland, 2014a.
- Winstroth, J. and Seume, J. R.: Wind Turbine Rotor Blade Monitoring Using Digital Image Correlation: 3D Simulation of the Experimental  
395 Setup, EWEA 2014, 10-13 March 2014, Barcelona, Spain, 2014b.
- Winstroth, J. and Seume, J. R.: Error Assessment of Blade Deformation Measurements on a Multi-Megawatt Wind Turbine Based on Digital Image Correlation, Proceedings of the ASME Turbo Expo, GT2014-43622, 2015.
- Winstroth, J., Schoen, L., Ernst, B., and Seume, J. R.: Wind Turbine Rotor Blade Monitoring Using Digital Image Correlation: A Comparison to Aeroelastic Simulations of a Multi-Megawatt Wind Turbine, Journal of Physics: Conference Series, 524 012064, 2014.
- 400 Wiser, R., Jenni, K., Seel, J., Baker, E., Hand, M., Lantz, E., and Smith, A.: Forecasting Wind Energy Costs and Cost Drivers: The Views of the World's Leading Experts, Tech. rep., IEA Wind Task 26, 2016.
- Wu, R., Zhang, D., Yu, Q., Jiang, Y., and Arola, D.: Health monitoring of wind turbine blades in operation using three-dimensional digital image correlation, Mechanical Systems and Signal Processing, 130, 470–483, <https://doi.org/10.1016/j.ymssp.2019.05.031>, 2019.